CRYSTAL GROWTH & DESIGN

Article

pubs.acs.org/crystal

Rigid Core Anthracene and Anthraquinone Linked Nitronyl and Iminoyl Nitroxide Biradicals

Handan Akpinar,[‡] John A. Schlueter,[§] Rafael A. Allão Cassaro,[#] Jonathan R. Friedman,[∥] and Paul M. Lahti*[,‡]

[‡]Department of Chemistry, University of Massachusetts, Amherst, Massachusetts 01003, United States

[§]Division of Materials Research, National Science Foundation, 4201 Wilson Boulevard, Arlington, Virginia 22230, United States

[#]Instituto de Química, Universidade Federal do Rio de Janeiro, Rio de Janeiro, RJ 21945-970, Brazil

[∥]Department of Physics and Astronomy, Amherst College, Amherst, Massachusetts 01002, United States

Supporting Information

ABSTRACT: The first syntheses of bis(nitronyl nitroxide) and bis(iminoyl nitroxide) (diNN, diIN) biradicals linked through rigid acene core conjugating anthracene (A) and anthraquinone (AQ) units are reported. Computational modeling predicts weak intramolecular exchange in AQ-linked systems, but A-linked biradicals to have ground state multiplicities consistent with the Borden-Davidson disjointness model. Solution electron spin resonance spectra showed inter-radical exchange-coupled triplet states, except for 2,6-AQ biradicals showing isolated spin spectra. Crystallography of the A-linked biradicals shows a key role for inter-radical contacts for molecular packing. DiINs showed lower-dimensional dyad packing with disorder at the radical units: the conformationally more symmetrical diNNs gave staircase one-dimensional or brickwork two-dimensional lattices. Core anthracene unit stacking was only seen in two systems with bromine on the central anthracene ring: the (large) bromine occupies alternate side placement in dyad stacks for the diIN, chain stacks for the diNN. Magnetism of 2,7-A-linked systems showed predominant ferromagnetic intramolecular triplet-singlet splitting of 24−28 K for diNNs and 8 K for diINs, plus weak antiferromagnetic (AFM) interactions from intermolecular contacts. The 2,6-A-linked biradicals showed AFM exchange between spins. Both A and AQ cores offer possibilities for electronic material development, with a combination of multiple radical spins and π-electron-rich acene cores.

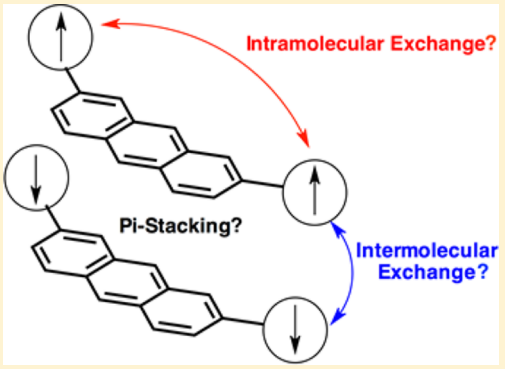

1. INTRODUCTION

Since the 1800s, there has been interest in understanding structure−property relationships for non-Kekulé molecules, which have sufficient atoms but insufficient bonds when standard rules of valence are applied.[1−3] A topic of particularly intense pursuit has been the dependable prediction of ground state spin multiplicity as a function of qualitative molecular connectivity and spin parity for polyradicals and related open-shell systems. Theoretical models such as those by Ovchinnikov,[4] by Klein,[5] and by Borden and Davidson[6] were eventually matched by experimental methodologies to probe ground spin states.

A promising recent offshoot of such investigations is the possibility of making multifunctional materials[7] where spin exchange and other electronic properties are both modulated. Examples include metal-free magnets[8] and photochemically switchable[9,10] or spintronic[11−13] behaviors in open-shell organic systems. Conjugated polycyclic aromatic and extended acene systems could be very useful for multipurpose electronic design because they can absorb light strongly, have extended spin-polarizable pi-electron networks, and have structural rigidity that can give intermolecular pi-stack interactions. However, despite intense study of conjugated multiradicals, only limited attention has been paid to molecular systems with multiple radical spin units linked by rigid polycyclic aromatics or longer acene units.

Berson's group reported ground-breaking matrix isolation studies[14,15] of anthracene-based non-Kekulé molecules I and II (Scheme 1) and studied their ground-state multiplicities with regard to expectations of spin polarization parity models. Such systems are too reactive for use as organic electronic materials: for practical use, stable radical units are desirable. For example, Sugawara's group described[15] the syntheses of III−IV with weak and qualitatively different inter-radical exchange in accord with spin polarization in the linker units: the thianthrenyl groups could be oxidized to provide an additional spin-state modulation route. More recently, Baumgarten and co-workers reported[16] promising computational and experimental studies

Received: April 17, 2016
Revised: May 11, 2016
Published: May 26, 2016

DOI: 10.1021/acs.cgd.6b00588
Cryst. Growth Des. 2016, 16, 4051−4059

Scheme 1. Example Polycyclic Aromatic-Linked Multiradicals

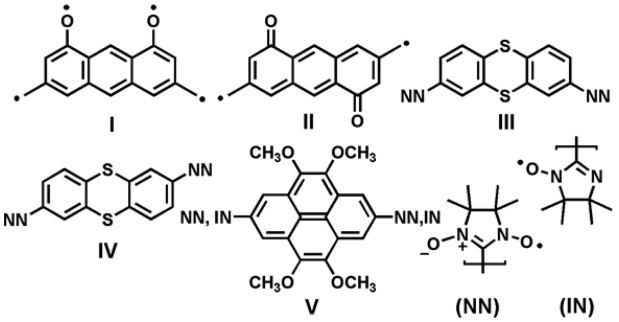

of biradicals V linked by a 2,7-pyrenediyl, an excellent example for multifunctional addressing of properties such as absorption, luminescence, redox, and spintronic behavior. Also recently, Hui and Chandresekar reported using macrocycles functionalized as bis(verdazyl) biradicals to self-assemble into microtubular light pipes.[17]

Although Ali and Datta reported computational modeling[18] of some bis(nitronyl nitroxide)s linked by polycyclic aromatics, syntheses of such biradicals linked by acene units remain lacking. Recently, some of us reported the study of an anthraquinone nitronyl nitroxide.[19] We now extend this work to report the syntheses of the first bis(nitronyl nitroxide = NN) and bis(iminoyl nitroxide = IN) biradicals having anthracene and anthraquinone-based spin-coupling core units. A combination of electron spin resonance (ESR) spectroscopy, computational modeling, and single crystal X-ray diffraction studies linked with solid state magnetic studies (for the most crystalline samples) provides structure−property relationships for interradical interaction as a function of connectivity, core spin-coupling unit, and radical spin unit. Moreover, the choice of spin unit plays an important role in determining the nature and dimensionality of intermolecular packing in the crystal lattice.

2. EXPERIMENTAL SECTION

2.1. General. Full synthetic details for the target biradicals—following the schemes in Figure 1—are given in the Supporting Information.

2.2. X-ray Crystallography. Crystallographic details were deposited with the Cambridge Crystallographic Data Centre (CCDC). The crystal structures of A26diNN and A26diIN were determined at the Advanced Photon Source (ChemMatCARS Sector 15 beamline). The former was determined from a twinned crystal having two components related by 180 deg rotation about reciprocal axis 1 0 0. Other structures were determined using a Bruker-Nonius CCD diffractometer at Amherst.

2.3. Magnetic Measurements. Magnetic measurements were carried out at the UMass Amherst Nanomagnetics Characterization Facility (Quantum Design MPMS-7 SQUID instrument), or at Amherst College (PPMS-9). Crushed polycrystalline samples in gelatin capsules were held in place with a small plug of cotton, mounted in a sample-holder, purged with helium, and cooled for measurements between 1.8 and 300 K of dc magnetic susceptibility (χ = magnetization/field = M/H). Raw susceptibility values were corrected for diamagnetic and sample holder contributions by extrapolation of the high-temperature data.

2.4. Materials. Syntheses of synthetic intermediates in Figure 1 have been previously reported for 2,7-dimethylanthracene,[20] 2,7-dimethylanthra-9,10-quinone,[20] 2,6-dimethylanthra-9,10-quinone,[20] dimethyl anthracene-2,7-dicarboxylate,[21] anthracene-2,6-dicarbaldehyde,[22] and 2,3-bis(*N*-hydroxylamino)-2,3-dimethylbutane hydrogen sulfate.[23]

*2,7-Bis(1-oxyl-3-oxo-4,4,5,5-tetramethylimidazolin-2-yl)-9-bromoanthracene (**BrA27diNN**).* Dark green needles, mp > 300 °C. MS (FAB): found m/z = 568.1714; calc for ($C_{28}H_{31}{}^{79}BrN_4O_4$ + 2 H) m/z = 566.16852. ESR (toluene, 9.6503 GHz): peak-to-peak splitting (ΔH_{pp}) = 3.9 gauss. CCDC deposition #1435878.

*2,7-Bis(1-oxyl-4,4,5,5-tetramethylimidazolin-2-yl)-9-bromo-anthracene (**BrA27diIN**).* Red solid. MS(FAB): found m/z = 536.1785,

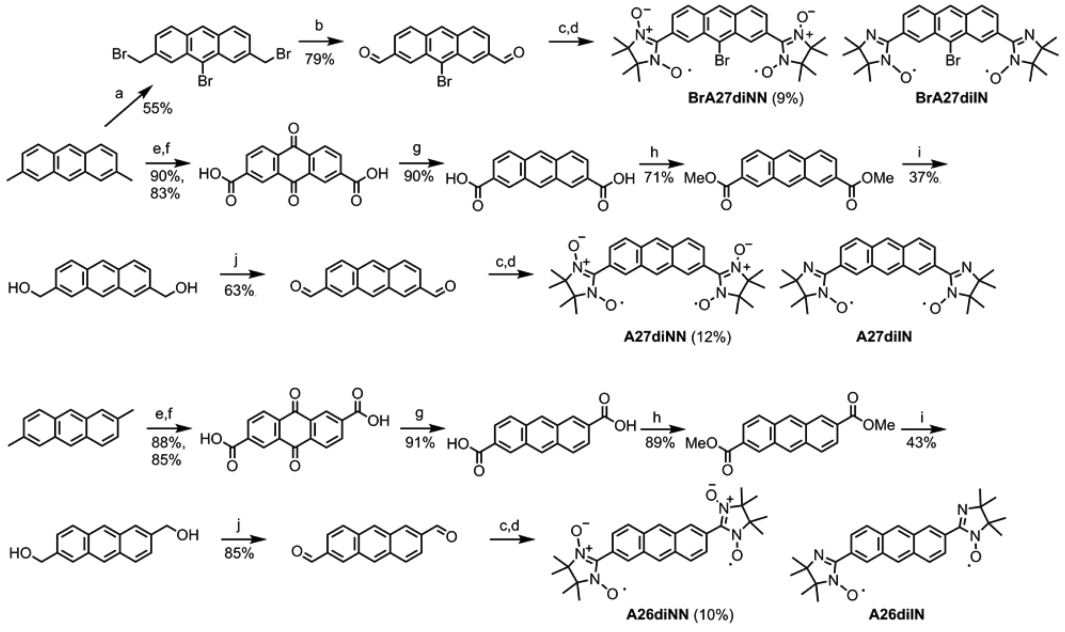

Figure 1. Synthesis of anthracene linked biradicals in this study. (a) 2 equiv of *N*-bromosuccinimide/CCl_4/boil; (b) 2-nitropropane/NaOEt/EtOH, 50 °C; (c) HO-NC(Me_2)-C(Me)$_2$-NOH·H_2SO_4, Et_3N, methanol-chloroform, boil, 48 h; (d) aq $NaIO_4$, CH_2Cl_2, 50 °C, 10 min; (e) CrO_3/H_2O/HOAc, boil; (f) $CrO_3/H_2SO_4/Ac_2O$/HOAc, heat; (g) Zn, conc NH_3(aq), heat; (h) CH_3I, Li_2CO_3, dry DMF, room temp; (i) $LiAlH_4/Et_2O$/0 °C, then H_2O; (j) MnO_2, CH_2Cl_2, room temp, 2 days.

DOI: 10.1021/acs.cgd.6b00588
Cryst. Growth Des. 2016, 16, 4051−4059

calc for ($C_{28}H_{31}{}^{79}BrN_4O_2$ + 2H) m/z = 536.16304. ESR (CH_2Cl_2, 9.5395 GHz): ΔH_{pp} = 4.4 gauss. CCDC deposition #1435877.

*2,7-Bis(1-oxyl-3-oxo-4,4,5,5-tetramethylimidazolin-2-yl)-anthracene (**A27diNN**).* Dark green needles, mp 244−246 °C. MS (FAB): found m/z = 488.2427, calc for $C_{28}H_{32}N_4O_4$ m/z = 488.2424. ESR (toluene, 9.6171 GHz): ΔH_{pp} = 3.5 G.

*2,7-Bis(1-oxyl-4,4,5,5-tetramethylimidazolin-2-yl)anthracene (**A27diIN**).* Red solid. MS (FAB): found m/z = 456.25161, calc for $C_{28}H_{32}N_4O_2$ m/z = 456.25252.ESR (toluene, 9.6047 GHz): ΔH_{pp} = 2.3, 4.4 gauss. CCDC deposition #1435876.

*2,6-Bis(1-oxyl-3-oxo-4,4,5,5-tetramethylimidazolin-2-yl)-anthracene (**A26diNN**).* Dark green needles from dichloromethane/acetonitrile, mp 238−240 °C. MS (FAB): found m/z = 488.2416, calc for $C_{28}H_{32}N_4O_4$ m/z = 488.24236. ESR (toluene, 9.6490 GHz): ΔH_{pp} = 3.9 gauss. CCDC deposition #1435875.

*2,6-Bis(1-oxyl-4,4,5,5-tetramethylimidazolin-2-yl)anthracene (**A26diIN**).* Red solid. MS (FAB): found m/z = 456.2634, calc for $C_{28}H_{32}N_4O_2$ m/z = 456.25253. ESR (toluene, 9.4968 GHz): ΔH_{pp} = 2.3, 4.3 gauss. CCDC deposition #1435874.

*2,7-Bis(1′-oxyl-3′-oxo-4′,4′,5′,5′-tetramethylimidazolin-2′-yl)-9,10-anthraquinone (**AQ27diNN**).* Brown powder, mp 260−270 °C; solutions are green, but after a few days turn brown. MS (FAB): found m/z = 519.2230, calc for ($C_{28}H_{30}N_4O_6$+H) m/z = 519.2244; found m/z = 518.2165, calc for $C_{28}H_{30}N_4O_6$ m/z = 518.2165. IR (neat, cm^{-1}; C═O stretch): 1727 (wk), 1684 (str). ESR (toluene, 9.6168 GHz): ΔH_{pp} = 3.6 gauss.

*2,7-Bis(1′-oxyl-3′-oxo-4′,4′,5′,5′-tetramethylimidazolin-2′-yl)-9,10-anthraquinone (**AQ27diIN**).* Red solid. MS (FAB): found m/z = 487.2338, calc for ($C_{28}H_{30}N_4O_4$ + H) m/z = 487.23453; found m/z = 486.1858, calc for $C_{28}H_{30}N_4O_4$ m/z = 486.22745. IR (neat, cm^{-1}; C═O stretch): 1725 (wk), 1680 (str). ESR (toluene, 9.6148 GHz): ΔH_{pp} ≈ 2.3, 4.3 gauss (poorly resolved).

*2,7-Bis(1-oxyl-3-oxo-4,4,5,5-tetramethylimidazolin-2-yl)-9,10-anthraquinone (**AQ26diNN**).* Brown powder, mp 215−220 °C. MS (FAB): found m/z = 518.2169, calc for $C_{28}H_{30}N_4O_6$ m/z = 518.21653. IR (neat, cm^{-1}; C═O stretch): 1725 (str), 1676 (str). ESR (toluene, 9.6051 GHz): ΔH_{pp} = 7.3 gauss.

*2,7-Bis(1-oxyl-4,4,5,5-tetramethylimidazolin-2-yl)-9,10-anthraquinone (**AQ26diIN**).* Red solid. MS (FAB): found m/z = 488.2437, calc for ($C_{28}H_{30}N_4O_4$ + 2H) m/z = 488.24236. IR (neat, cm^{-1}; C═O stretch): 1728 (str), 1677 (str). ESR (toluene, 9.6068 GHz): ΔH_{pp} = 4.6, 8.9 gauss.

3. RESULTS AND DISCUSSION

3.1. Choice of Target Biradical Structures. The alternant, nondisjoint [6] π-connectivity parity of anthracen-2,7-diyl (A27) should induce ferromagnetic (FM) exchange coupling between spin units, based on spin polarization expectations as shown in Scheme 2. Anthracen-2,6-diyl (A26) is disjoint in the Borden-Davidson sense,[6] with antiferromagnetic (AFM) coupling expected, though high or low spin ground states can arise[3] from small structural variations in disjoint systems. Similarly, anthraquinone-2,7-diyl (AQ27) and anthraquinone-2,6-diyl (AQ26) linker units are nondisjoint and disjoint, respectively.

Scheme 2. Expected Spin Polarization Parities for A27 and A26 Units Linking Two Spin Units (Broken Circles)[a]

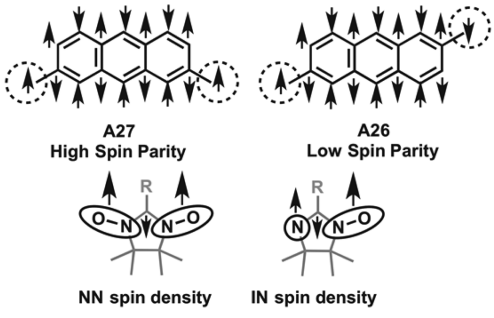

[a]Qualitative radical spin polarizations are shown.

The NN and IN spin units in the biradicals are directly linked to the acene cores at sites of low spin density (Scheme 2, lower row). Thus, exchange coupling between radicals might be decreased, relative to situations where large spin density sites are directly linked to the core, like I−II in Scheme 1. Still, di-NN and di-IN biradicals linked through smaller, 1,3-phenylene units usually (not always[3]) give triplet states.[24,25]

3.2. Synthesis of Anthracene-Core Biradicals. Figure 1 shows syntheses of the biradicals made for this study. Benzylic bromination of 2,7-dimethylanthracene gave unavoidable bromination of the central anthracene ring. The resulting tribromide could be converted to a dialdehyde, but efforts to reductively remove the bromine or directly oxidize the dimethylanthracene to a dialdehyde gave product mixtures. Oxidation of 2,7- or 2,6-dimethylanthracene gave anthraquinone dicarboxylic acids that were converted to anthracene dicarbaldehydes as shown.

The dialdehydes were condensed with 2,3-bis(*N*-hydroxylamino)-2,3-dimethylbutane to make the radical precursor bis(*N*-hydroxyl)imidazolines, which were oxidized with aqueous sodium periodate[23] to give di-NNs as major products, sometimes with small amounts of di-IN byproducts. These were readily separated by column chromatography as dark green solids and blood-red solids, respectively. Structure assignments were made by mass spectrometry and ESR spectroscopy, bolstered by X-ray diffraction (XRD) studies when good quality single crystals were isolated. No mixed IN-NN biradicals were isolated.

3.3. Synthesis of Anthraquinone-Core Biradicals. Figure 2 shows the syntheses of the anthraquinone (AQ) linked biradicals. Precursor dialdehydes were functionalized[23] to bis(*N*-hydroxyl)imidazoline rings and oxidized to give mixtures of di-NN and di-IN products that were separated by column chromatography as brown and deep red solids, respectively. The compounds were identified by mass spectrometry, ESR spectroscopy, and infrared spectroscopy. Unfortunately, none of the AQ-linked biradicals gave diffraction

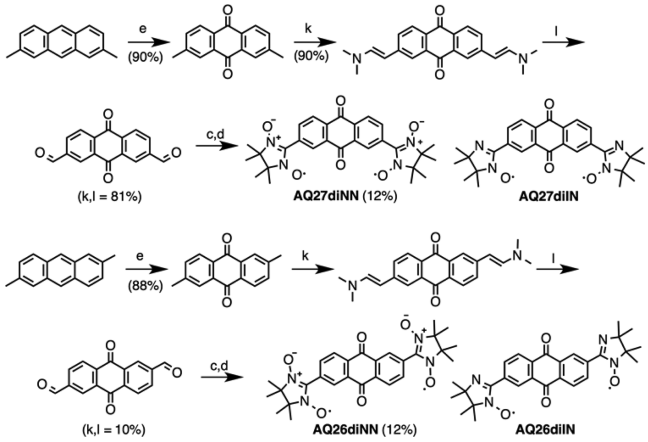

Figure 2. Synthesis of anthraquinone linked biradicals in this study. (c) HONH-$C(Me_2)$-$C(Me)_2$-NHOH·H_2SO_4, Et_3N, methanol−chloroform, boil, 48 h; (d) aq $NaIO_4$, CH_2Cl_2, 50 °C, 10 min; (e) CrO_3/H_2O/HOAc, boil; (k) $HC(OMe)_2NMe_2$, DMF, boil, 24 h; (l) $NaIO_4/H_2O$/THF, room temp, 1 h.

DOI: 10.1021/acs.cgd.6b00588
Cryst. Growth Des. 2016, 16, 4051−4059

Table 1. Single Crystal Structure X-ray Diffraction Data Collection and Refinement Parameters for Biradicals in This Study

compound	BrA27diNN	BrA27diIN	A27diIN	A26diNN	A26diIN
empirical formula	$C_{28}H_{31}N_4O_4Br$	$C_{28}H_{31}N_4O_xBr$ [x = 1.67, 0.17(O2B)]	$C_{28}H_{32}N_4O_2$	$C_{28}H_{32}N_4O_4$	$C_{28}H_{32}N_4O_2$
formula weight (g·mol^{-1})	567.47	535.47	456.58	488.58	456.58
temperature (K)	293	293	293	95	95
X-ray source	Sealed	Sealed	Sealed	Synchrotron	Synchrotron
wavelength (Å)	0.71073	0.71073	0.71073	0.39360	0.39360
crystal system	orthorhombic	monoclinic	tetragonal	monoclinic	monoclinic
space group	*Pbcn*	$P2_1/n$	$I\bar{4}$	$P2_1/c$	$P2_1/n$
axes (Å)	a = 19.3108(4)	a = 7.4926(1)	a = 27.156(4)	a = 9.5582(6)	a = 6.3636(3)
	b = 18.8674(4)	b = 18.2682(4)	b = 27.156(4)	b = 12.6106(7)	b = 10.7038(5)
	c = 7.2850(1)	c = 19.5485(4)	c = 6.8023(14)	c = 10.9435(6)	c = 17.6698(9)
β (deg)	90.00	100.4044(11)	90.00	111.566(1)	93.347(1)
volume (Å^3)	2654.25(9)	2631.73(9)	5016.4(18)	1226.73(12)	1201.52(10)
Z	4	4	8	2	2
calculated density (g cm^{-3})	1.420	1.352	1.209	1.323	1.262
absorption coefficient (mm^{-1})	1.590	1.594	0.077	0.037	0.081
F(000)	1176	1112	1952	520	488
index ranges	h = −22→22	h = −8→8	h = −32→32	h = −15→14	h = −7→9
	k = −22→22	k = −21→20	k = −22→22	k = −0→21	k = −15→15
	l = −8→8	l = −23→23	l = −8→6	l = −0→18	l = −26→25
reflections collected	4335	8635	4055	58680	26547
restraints/parameters	0/169	0/326	45/389	0/164	0/308
goodness-of-fit on F^2	1.125	1.044	1.008	0.998	1.065
R_1, wR_2, [$I > 2\sigma(I)$]	0.0434, 0.0951 (1887)	0.0631, 0.1755 (3786)	0.0481, 0.1183 (4055)	0.05030, 1152 (4520)	0.0565, 0.1515 (2761)
R_1, wR_2, (all data)	0.0607, 0.0951 (2341)	0.0764, 0.1874 (4625)	0.0673, 0.1320 (4055)	0.0773, 0.1291 (5969)	0.0837, 0.1775 (3845)
$\Delta\rho_{min}$, $\Delta\rho_{max}$, (e·Å^{-3})	−0.48, 0.47	−0.39, 1.19	−0.12, 0.14	−0.38, 0.48	−0.17, 0.30
CCDC deposition no.	1435878	1435877	1435876	1435875	1435874

Table 2. Intermolecular Crystallographic Contacts between Radical π-Spin-Bearing Sites (O−N−C−N[−O] Units)[a]

compound	contact	value	compound	contact	value
BrA27diNN			BrA27diIN		
	O2···O2^{i}	3.655(5)		O1B···N3^{iv}	3.895(19)
	O2···O2^{ii}	3.655(5)		O1B···C18^{iv}	3.698(18)
	O2···N2^{ii}	3.390(5)		O2B···N3^{iv}	3.895(19)
	O2···C9^{ii}	3.680(4)		O2B···C18^{iv}	3.698(18)
A27diIN			A26diNN		
	O2···N4^{iii}	4.593(4)		O2···O2^{v}	3.6523(13)
	O2···C22^{iii}	4.230(5)		O2···N1^{v}	3.9338(14)
				O2···N2^{v}	3.5189(13)
				O1···N1^{vi}	3.9501(14)

[a]Symmetry operations used to generate the molecule in close contact: i = x, 2 − y, −1/2 + z; ii = x, 2 − y, 1/2 + z; iii = x, y, 1 + z; iv = 1 − x, −y, 1 − z; v = 2 − x, −y, −z; vi = 1 − x, −y, −z.

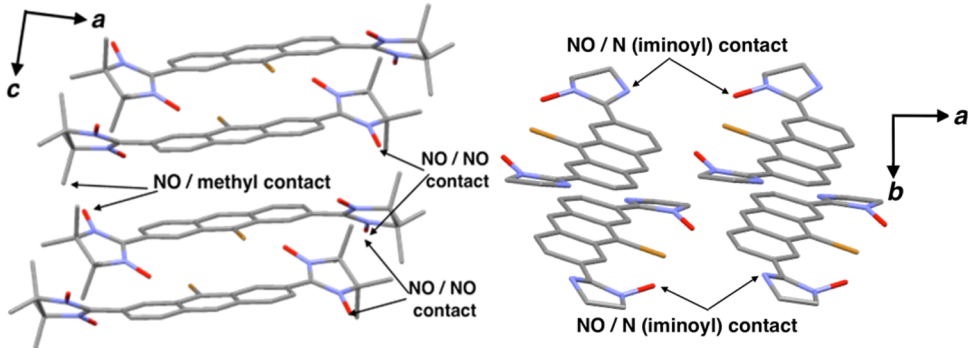

Figure 3. Intermolecular close contacts BrA27diNN (left) and BrA27diIN (right). Hydrogens and some methyl groups omitted for clarity.

DOI: 10.1021/acs.cgd.6b00588
Cryst. Growth Des. 2016, 16, 4051−4059

grade crystals, which precluded effective magnetostructural analysis of intermolecular solid state interaction between biradicals.

3.4. Crystallography. A Cambridge Structure Database search for NN or IN linked to anthracene or anthraquinone found 9-anthracene nitronyl nitroxide (9ANN[26]) and our previous report[19] of 2-anthraquinone nitronyl nitroxide. We could not obtain XRD quality crystals for any of the new AQ biradicals. The anthracene biradicals were more tractable, excepting A27diNN. Data collection and structure refinement parameters are given in Table 1, and select intermolecular close contacts are given in Table 2: an extended set of close contacts is listed in Table S1. ORTEP structure diagrams are given in Supporting Information, Figures S1−S5.

BrA27diNN and BrA27diIN crystallize with antiparallel stacking of acene cores (Figure 3). BrA27diNN has 1-D chains of acene units stacked along the *c*-axis 3.5 Å apart, with C−Br bonds in alternating positions. BrA27diIN does *not* form extended stacks, but rather dimers along the *b*-axis, again with antiparallel C−Br orientation. This cofacial π-stacking of anthracene units is similar to that in 9ANN, with the large substituents on the 9-position on alternating, sides of π-stacked units. The Br-substituent induces cofacial π-stacking and optimized lattice space utilization by placement alternating sides of the stack, as seen in biradical 5-iodo-1,3-phenylene-bis(nitronyl nitroxide).[27] A number of anthracenes with sizable but simple 9-substituents show such alternation, including 9ANN: see a listing in Supporting Information, Crystal Search S1.

Chains of N−O to methyl group contacts between BrA27diNN NN units help assemble the acene stacks (Figure 3, left, *c*-axis). BrA27diIN has only one N−O group per IN unit, limiting the number of possible N−O to methyl contacts compared to BrA27diNN: this probably is the reason for π-stacked dimer formation instead of chain formation in the diIN. The BrA27diNN 1-D chains have N−O···O−N inter-radical contacts along the *c*-axis with r(O2···O2^{i}) = 3.655(5) Å (Figure 3, Table 2). These inter-radical contacts are moderately close, but the N−O units are quite canted to one another, limiting overlap between singly occupied molecular orbitals (SOMOs). BrA27diIN also forms chains of N−O to iminoyl nitrogen inter-radical contacts along the *b*-axis with r(O1B···N3^{iv}) = 3.895(19) Å, with acene staircase stacking along the *a*-axis. The inter-radical contacts between the Br27diIN staircase stacks also have strong canting of N−O units relative to one another: the combination of longer inter-radical distance and canting should further limit SOMO−SOMO overlap.

Despite numerous efforts, we could not obtain diffraction grade crystals for A27diNN, but A27diIN forms crystals having staircase stacks of core acenes, parallel to the *c*-axis (Figure 4), with 1-D chains of N−O2 to iminoyl nitrogen inter-radical contacts. Only one IN unit per A27diIN forms the inter-radical contacts, which are similar but much longer than the analogous contacts in BrA27diIN, r(O2···N4^{iii}) = 4.593(4) Å. The other IN group in A27diIN forms N−O to methyl and methyl to π-cloud contacts with other acene units. The result is a set of four staircase stacks associated by complementary IN methyl group to acene π-electron contacts (see Supporting Information, Figure S6).

A26diNN forms various N−O to methyl contacts (Figure 5), as well as inter-radical N−O···O−N contacts between high spin density sites. The NN units interdigitate alternately between acene units, and form 2-D brickwork packing in the *ac*-plane.

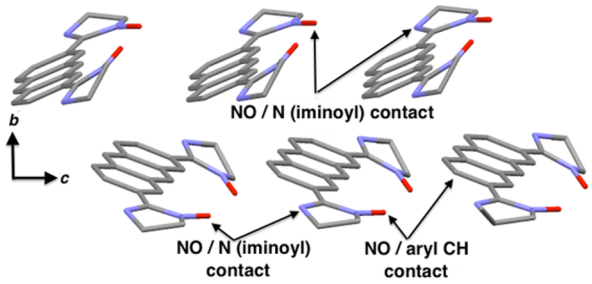

Figure 4. Intermolecular close contacts in A27diIN. Methyl groups, disordered atoms, and hydrogens omitted for clarity.

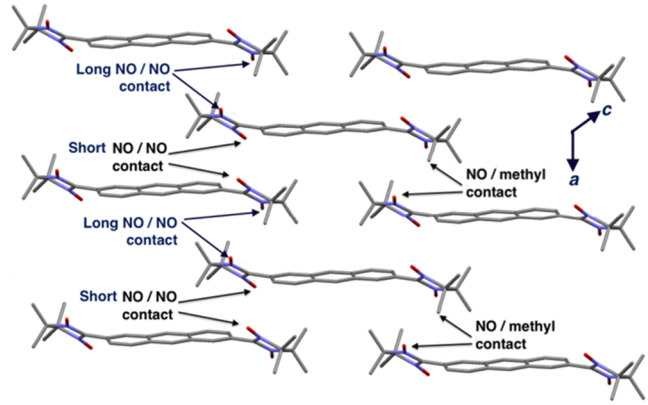

Figure 5. Intermolecular brickwork packing and inter-radical close contacts in A26diNN. Hydrogens omitted for clarity.

The N−O···O−N contacts are alternating chains with *r*(O2···O2^{v}) = 3.6523(13) Å, and r(O1···O1^{vi}) = 4.0837(13) Å. The closest N−O2···^{v}O2−N contacts are important to understand the magnetism of A26diNN, as discussed below.

A26diIN has whole molecule lattice disorder, plus rotational disorder in one IN spin units. Its core acene rings are strongly slip-stacked along the acene long axis, and staircase stacked along the *b*-axis (see Supporting Information, Figure S7). Inter-IN, dyad-type N−O to methyl contacts link the acene cores into a herringbone array in the *bc*-plane (Figure 6). These do *not* give direct contacts between high spin density sites, so strong inter-radical exchange interactions are not expected here (see below). However, inter-radical N−O···H−C (radical methyl) contacts provide possible pathways for dipole−dipole or weak spin-polarized exchange interaction, as discussed below.

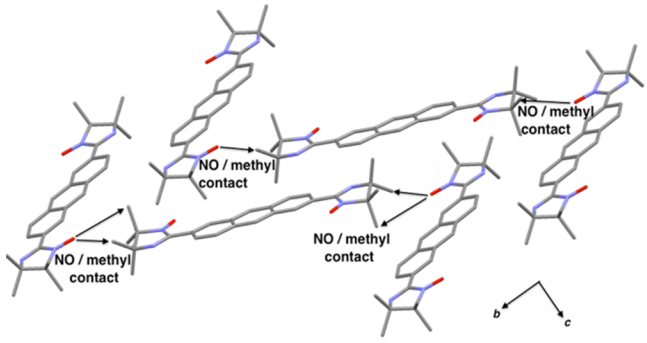

Figure 6. Intermolecular close contacts in A26diIN: a herringbone acene array linked by inter-IN contacts (bottom). Disordered atoms and hydrogens omitted for clarity.

DOI: 10.1021/acs.cgd.6b00588
Cryst. Growth Des. 2016, 16, 4051−4059

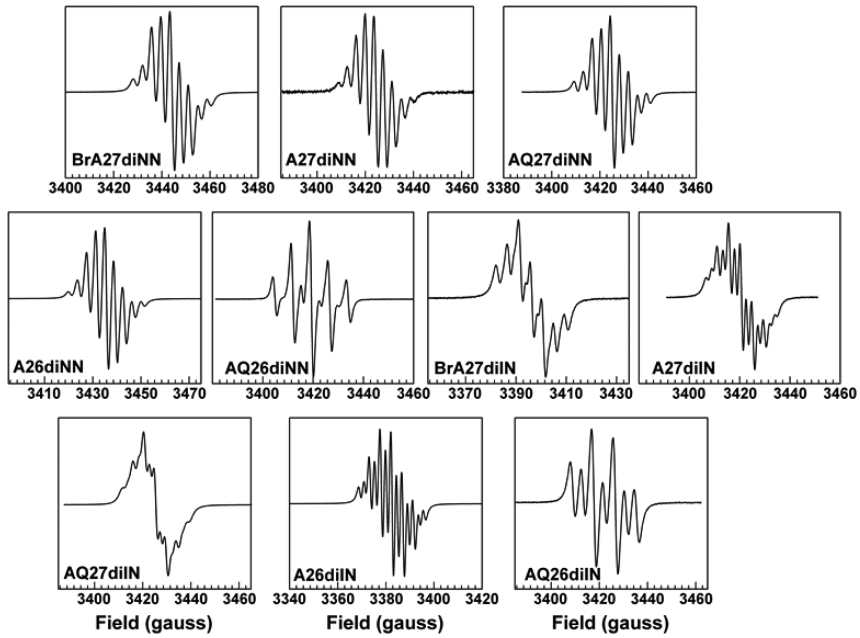

Figure 7. Room temperature solution ESR spectra; BrA27diNN, 9.6503 GHz; A27diNN, 9.6171 GHz; AQ27diNN, 9.6168 GHz; A26diNN, 9.6490 GHz; AQ26diNN, 9.6051 GHz; BrA27diIN, 9.5395 GHz; A27diIN, 9.6047 GHz; AQ27diIN, 9.6148 GHz; A26diIN, 9.4968 GHz; AQ26diIN, 9.6068 GHz.

3.5. Intramolecular Exchange from ESR Studies. The ESR solution spectra at room temperature (Figure 7) for nondisjoint di-NNs BrA27diNN, A27diNN, and AQ27diNN showed well-resolved nine-line spectra, with peak intensities and shapes indicating triplet-singlet exchange coupling much greater than the N-14 hyperfine coupling (hfc), $J \gg a_N$. For such biradical spectra, the peak-to-peak splitting (ΔH_{pp}) is half the value of the hfc, yielding a_N = 7−8 gauss (4−5 mJ/mol) for two nitrogens in these diNNs, which is typical for nitronyl nitroxides. Spectral line shape simulations[28] deviated noticeably from these nine-line patterns when J < 55 mJ/mol (J/k = 6.7 mK). We take this as the *lower limit* for exchange interaction between the NN units in solution to give a triplet state.

The disjoint, anthracene-linked biradical A26diNN also showed a nine-line ESR spectrum in solution at room temperature (Figure 7), but AQ26diNN showed essentially a five-line solution ESR spectrum with ΔH_{pp} = 7.3 gauss like that of a NN monoradical. The latter case is consistent with the AQ26 unit giving almost no effective exchange between NN units. Mass spectrometry of AQ26diNN supports the biradical structure, but a double-integrated, solution ESR spin count AQ26diNN was somewhat lower than expected for two spins. Aggregation of the biradicals into chains with AFM interaction between spins (except on chain ends) may cause this spin count result, as suggested by Kanzai et al.[29] for similar behavior of a bis-TEMPO biradical.

The di-IN systems A27diIN and A26diIN both gave room-temperature solution ESR spectra (Figure 7) that both showed 13 distinct lines with ΔH_{pp} about one-half of the hfc in mono-IN spectra, consistent with triplet biradicals having inter-IN triplet exchange with $J \gg a_N$ where a_N = 4.2 and 9.2 G. The BrA27diIN and AQ27diIN spectra are line-broadened in comparison to the A27 and A26 di-IN biradicals. The line-broadening could arise due to equilibration between multiple di-IN conformations in solution, but could also occur if $J \approx a_N$, with smaller inter-radical exchange than in the other di-INs, or also if J grows large enough for strong relaxation effects to cause broadening. As described below, computational modeling indicates that anthraquinone linked biradicals have *smaller* interspin exchange than the analogous anthracene-linked systems.

Freezing the biradical solutions at 77 K in all cases gave ESR spectra dominated by an intense single peak in the $g \approx 2$ region (see Supporting Information, Figure S8). Strong AFM spin pairing with a robust singlet state would show no ESR signal, but the samples all show strong ESR signals at 77 K. There are no clearly resolved triplet zero-field splitting (zfs) features in the frozen solution temperature spectra, although some spectra show shoulder features or broadening on the main peak that could be due to perpendicular triplet spectral turning points, or to anisotropic hyperfine coupling from the radical nitrogen atoms. In either case, the zfs should roughly be no more than the $g \approx 2$ region line widths at half height, which are ∼50 gauss. Given the distance between radical spin units, small spin density presumed on the acene, and broadening effects of nitrogen hyperfine, the lack of resolved zfs in the spectra is not surprising. A simple dipolar interaction estimate using NN units at the crystal geometry of BrA27diNN, with computed spin densities, predicts zfs of ∼23 gauss. No triplet half-field ESR transitions were seen, but these can be weak for small zfs.

Overall, the ESR experiments indicate that the anthracene-coupled biradicals have triplet ground or thermally accessible states, whether nondisjoint or disjoint. The formally non-disjoint anthraquinone biradicals show analogous behavior, but the disjoint anthraquinone biradicals have essentially non-interacting radical spin units consistent with very weak exchange, if any.

3.6. Intramolecular Exchange from Computational Modeling. Berson's studies of I and II (Scheme 1)[14] showed ground spin states in accord with semiempirical[30] computational studies. Ali and Datta used applied hybrid density functional theory (DFT) level UB3LYP/6-311+G(d,p) computations for some bis-NN biradicals linked by polycylic aromatic core units, including A27diNN that was predicted[18] to be a

DOI: 10.1021/acs.cgd.6b00588
Cryst. Growth Des. 2016, 16, 4051−4059

Table 3. Computational Intramolecular Exchange Energies for Biradicals in This Study, with Experimental Comparisons

compound	computed E_T[a] (<S^2>)	computed E_S[b] (<S^2>)	computed $\Delta E(T-S)$[c] (J_{intra}/k[d])	experimental $J_{intra}/k(\theta)$[e]
BrA27diNN	−3862.781722(2.039)	−3862.781696(1.036)	69 J/mol (8.3 K)	28 K (−3.0 K)
A27diNN	−1290.540739(2.044)	−1290.540691(1.040)	125 (15.0)	24 K (−3.5 K)
A27diIN	−1140.273823(2.021)	−1140.273720(1.019)	30 (3.7)	7.9 K (−1.8 K)
A26diNN	−1290.540724(2.039)	−1290.540835(1.046)	−294 (−35.4)	strong AFM by magnetism[f]
A26diIN	−1140.273696(2.019)	−1140.273720(1.021)	−63 (−7.6)	−4.5 K (−3.8 K)
AQ27diNN	−1439.701644(2.042)	−1439.701654(1.042)	−27 (−3.2)	(triplet solution ESR)
AQ27diIN	−1289.432887(2.021)	−1289.432890(1.021)	−6.0 (−0.7)	(triplet solution ESR)
AQ26diNN	−1439.701717(2.042)	−1439.701715(1.042)	6.8 (0.8)	(isolated spin solution ESR)
AQ26diIN	−1289.432907(2.021)	−1289.432908(1.042)	−2.7 (−0.3)	(isolated spin solution ESR)

[a]UB97*D*/6-31G(d) energy in hartrees (spin-squared expectation value), geometry optimized. [b]UB97*D*/6-31G(d) energy in hartrees (spin-squared expectation value), at triplet state frozen geometry with broken symmetry wave function. [c,d]Computed triplet-singlet state energy in J/mol (K), with Yamaguchi correction (ref 33); triplet state is lower for positive values. [e]Experimental intramolecular exchangeJ_{intra}/k (mean field) from magnetic measurements; where unavailable, qualitative evaluations given. [f]Magnetic moment measurements small and variable in solid state.

ground triplet state by $\Delta E(T-S)$ = 161 J/mol, or $J_{intra}/k \approx$ 19.4 K for Hamiltonian $H = -J{\cdot}S_1S_2$.

Using Gaussian 09,[31] UB97D[32]/6-31G(d) computational predictions of ΔE(T-S) were used to assess the following effects on interspin exchange: (1) nondisjoint 2,7-connectivity versus disjoint 2,6-connectivity; (2) anthracene versus anthraquinone linkage; (3) NN vs IN spin-unit usage. Triplet states were geometry optimized, and this geometry frozen to compute the corresponding singlet state energy with a broken-symmetry wave function. Computed state energies and $\Delta E(T-S)$ gaps are given in Table 3, including corrections by Yamaguchi's method.[33]

Because singlet state geometries were not optimized, singlets could lie even lower in energy relative to triplets: we considered this approximation sufficient to determine trends. For example, we found computational $\Delta E(T-S)$ = 125 J/mol or J_{intra}/k = 15 K for A27diNN, compared to Ali and Datta[18] with J_{intra}/k = 19.4 K: both are in reasonable accord with the experimental J/k = 24 K in Table 1. The computations also support the magnetism results showing smaller singlet−triplet splitting in bis-IN versus bis-NN systems. UB3LYP[34,35]/6-31G* computations gave similar trends, but significantly larger exchange values (Supporting Information, Table S2).

The computations indicate low-spin ground states for all of the AQ-linked biradicals except AQ26diNN. The AQ27-linked biradicals show triplet ESR solution spectra, but these can arise from thermal population of low-lying triplet states. The AQ26 biradicals are experimentally different in showing no ESR evidence of a triplet state, but instead show spectra like isolated radicals. This behavior likely arises from a combination of factors in the AQ26 biradicals that each inhibit effective interspin-unit exchange: (1) poor exchange in biradical linker units through pathways that involve carbonyl units (considered to result in poor[36] inter spin-unit exchange); (2) disjoint connectivity of the AQ26 biradicals that disfavors high spin states; (3) poor exchange coupling through low spin density at the radical 2-position in the disjoint connectivity.

3.7. Intramolecular and Intermolecular Exchange from Magnetic Studies. Because we obtained no crystal structures for the anthraquinone biradicals, only anthracene core biradicals were subjected to solid-state magnetic studies. Variable-temperature magnetic susceptibility ($\chi = M/H$) versus temperature (T) were carried out, and the resulting data are shown as χT versus T plots in Figure 8. All of the biradicals were considered as two-spin systems using the Hamiltonian H

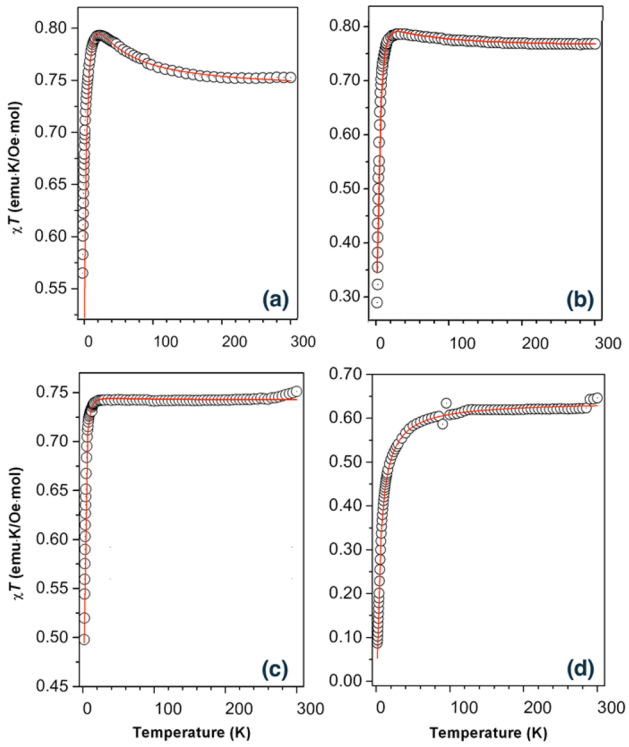

Figure 8. Magnetic χT vs T measurements for BrA27diNN (a), A27diNN (b), A27diIN (c), A26diIN (d) in a 1000 Oe dc external field, 1.8−300 K; solid lines are fits to eq 1.

$= -J_{intra}{\cdot}S_1S_2$, where $S_1 = S_2 = 1/2$. The data were fitted to a two-spin interaction model, eq 1,[37]

$$\chi T = \frac{2Ng^2\beta^2}{3k}\frac{1}{3+\exp(-J/kT)} \times \frac{T}{(T-\theta)} \quad (1)$$

where J_{intra}/k is intramolecular inter-radical exchange (triplet-singlet gap $\Delta E(T-S)$ in the biradical), and θ is a generalized mean-field term for any intermolecular exchange interactions; J_{intra}/k, θ, and the Landé g factor were fitted parameters: the other terms are constants with the usual meanings. The fitted parameters are given in Table 3.

All of the biradicals show AFM downturns in χT versus T at low temperatures (Figure 8), such that the mean fields $\theta < 0$ (Table 3). We attribute the AFM mean fields to inter-radical close contacts (see below). The dominant interspin interactions in the nondisjoint biradicals have $J_{intra}/k > 0$, attributable to

DOI: 10.1021/acs.cgd.6b00588
Cryst. Growth Des. 2016, 16, 4051−4059

intramolecular FM exchange expected for nondisjoint connectivity. The similar magnitudes of J_{intra}/k for BrA27diNN and A27diNN are consistent with linkage through similar anthracene-2,7-diyl linkers. Here, we are assuming near isolation of the A27diNN radicals in the solid, despite the lack of crystallographic proof, but the similar magnetic exchange is consistent with this assumption.

Attributing J/k to the same nondisjoint intramolecular mechanism, in A27diIN the two IN radicals are also FM exchange coupled, but more weakly than in the bis-NN system. By contrast, the IN radicals in A26diIN are AFM exchange coupled in accord with its disjoint connectivity. The A26diIN mean-field interaction is large compared to the fitted J_{intra}/k value, so the two-spin model of eq 1 does not apply as well as in the other cases, although it is physically reasonable. The quantitative results of magnetic fitting for disjoint A26diIN are thus somewhat uncertain, but qualitatively, are dominated by AFM exchange, quite unlike the nondisjoint 2,7-anthracenediyl-coupled biradicals.

Multiple attempts were made to study the solid-state magnetic behavior of A26diNN, with multiple samples. Magnetic moments were quite low and somewhat variable. Measurements for one sample yielded enough signal for a magnetization versus field (M vs H) plot to curve below the function of an isolated spins $S = 1/2$ Brillouin function (Supporting Information, Figure S9). In addition, for plots of M vs H/T (Supporting Information, Figure S10) data at 1.8 K lies below data at 4.0 K, suggesting a decreased value of χT at lower temperature. These indicate AFM interactions between spin sites and are not consistent with a robust triplet state. Sample decomposition might have occurred, although samples stored in a −10 °C freezer for over two years looked visually unchanged and gave the same ESR spectra as seen for new samples. The generally low magnetic response is consistent with strong AFM exchange across the particularly close, SOMO−SOMO overlapping contacts between NN spin sites in the crystallography of A26diNN (Figure 5). Because A26diNN gives a triplet ESR signal in solution, its expected disjoint AFM *intramolecular* exchange is apparently not strong enough to make the molecules diamagnetic. However, its *intermolecular* close contacts between high-spin-density sites in lattice arrangements that should favor spin AFM pairing, more than in any other compound of this study, would reasonably account for loss of magnetic moment. Further, the sum of results shows a strong difference in magnetic behavior between disjoint A26diNN and A26diIN, and the nondisjoint, 2,7-connectivity anthracene-linked biradicals.

For the magnetic results obtained, fitted exchange and mean-field terms are included in Table 2, with comparison to the computational modeling results for individual molecules. The magnetic exchange behaviors—where available—are qualitatively consistent with the Borden−Davidson model for ground-state spin multiplicity, and quantitatively show intramolecular NN exchange coupling to be stronger than between IN radicals. The strongest bulk-sample exchange is found in A26diNN, the only disjoint biradical (AFM *intramolecular* exchange expected) where *intermolecular* crystallography also shows good SOMO−SOMO overlapping contact between large spin density sites[38] on the radical O−N−C−N(−O) units. This SOMO−SOMO overlap will favor strong intermolecular AFM exchange. While BrA27diNN also has N−O···O−N contacts of ∼3.6 Å (Table 2, Supporting Information Table S1), its contacts have strong relative canting of the N−O groups, with poor inter-radical SOMO overlap that explains its modest mean field AFM exchange in Table 3. Similarly poor SOMO overlap at the N−O···O−N contacts in BrA27diIN, with its rotationally disordered IN units (Table S1), is also be expected to yield weak exchange.

The AFM mean field interactions $\theta < 0$ in Table 3 presumably arise due to various close contacts between atoms, at least one of which has small spin density. The N−O-to-methyl contacts in the biradicals likely provide such exchange pathways[39,40] by dipole−dipole or spin-polarized contacts involving low spin-density on the hydrogen atoms of the radical methyl groups. As described above, A26diNN has pathways for much stronger AFM exchange due to its good SOMO−SOMO overlap between large spin density sites, so any weaker interactions would not be readily discerned in A26diNN by bulk magnetic measurements.

4. CONCLUSIONS

The ground state multiplicities of 2,7- and 2,6-anthracenediyl linked nitronyl nitroxide and iminoyl nitroxide biradicals fit qualitative π-connectivity expectations. The large distances between spin units and limited spin delocalization give no resolvable ESR zfs, but solution spectra show triplet state formation in most of the biradicals. The anthraquinone-core biradicals are more weakly exchange coupled than anthracene-core analogues. These generalizations should help in designing similar biradicals.

Anthracene core π-stacking was only favored with a large substituent attached in the 9-position. However, staircase acene stacking in other cases gave relatively close association of the anthracene units, albeit with interactions between the radical units having a major influence on the final crystal packing, where single crystal formation allowed analysis. Various inter-radical N−O···O−N, N−O···H−C (radical methyl), and N−O···N (iminoyl) contacts in the biradical crystal lattices provide exchange interaction pathways. A26diNN gave a brickwork pattern of biradical packing that uniquely (in this set of molecules) produced close intermolecular contacts giving good SOMO−SOMO overlap to yield strong interaction between sites of high spin density. These findings should help with understanding and predicting molecular-lattice packing in structurally similar systems. Other stable radicals and biradicals connected to polycyclic acenes and aromatic systems should prove worthy targets of study, especially for electronic materials consideration.

■ ASSOCIATED CONTENT

Supporting Information

The Supporting Information is available free of charge on the ACS Publications website at DOI: 10.1021/acs.cgd.6b00588.

Full experimental details for syntheses and characterizations of biradicals; ORTEP diagrams of biradical crystal structures; brief summary of crystal structure search for 9-substituted anthracenes; table of intermolecular close contacts; table of computed singlet−triplet gaps in biradicals; frozen solution ESR spectra; magnetization versus field data for anthracene-core biradicals, archival computational output for biradical computations (PDF)

Accession Codes

CCDC 1435874−1435878 contain the supplementary crystallographic data for this paper. These data can be obtained free of

DOI: 10.1021/acs.cgd.6b00588
Cryst. Growth Des. 2016, 16, 4051−4059

charge via www.ccdc.cam.ac.uk/data_request/cif, or by emailing data_request@ccdc.cam.ac.uk, or by contacting The Cambridge Crystallographic Data Centre, 12 Union Road, Cambridge CB2 1EZ, UK; fax: +44 1223 336033.

AUTHOR INFORMATION

Corresponding Author

*E-mail: lahti@chem.umass.edu.

Author Contributions

H.A. synthesized all compounds and carried out basic characterizations, magnetic measurements, crystallization, multiple crystallographic analyses, and prepared experimental descriptions. J.A.S. carried out crystallographic measurements and analyses for A26diIN and A26diNN. JRF provided facilities, oversaw and assisted with magnetic analyses. R.A.A.C. carried out final crystallographic analysis for A27diIN. PML assisted with magnetic analyses and ESR spectroscopy, took main responsibility for manuscript preparation, and directed the project. All authors participated in preparation of the final manuscript.

Notes

The authors declare no competing financial interest.

ACKNOWLEDGMENTS

H.A. and P.M.L. thank the National Science Foundation for partial support of this work under Grant CHE-0809791. J.R.F. thanks the National Science Foundation for support under Grant No. DMR-1310135. The authors (J.A.S.) acknowledge with thanks the use of the Advanced Photon Source at Argonne National Laboratory: ChemMatCARS Sector 15 is principally supported by the Divisions of Chemistry (CHE) and Materials Research (DMR), National Science Foundation, under Grant Number NSF/CHE-1346572. Use of the Advanced Photon Source, an Office of Science User Facility operated for the U.S. Department of Energy (DOE) Office of Science by Argonne National Laboratory, was supported by the U.S. DOE under Contract No. DE-AC02-06CH11357. J.A.S. acknowledges support from the Independent Research/Development program while serving at the National Science Foundation.

DEDICATION

Dedicated to Jerome A. Berson for his 92nd birthday.

REFERENCES

(1) For a historical summary, see Berson, J. A. Meta-Quinonoid Compounds. In *The Chemistry of the Quinonoid Compounds*; Patai, S.; Zappoport, Z., Eds.; John Wiley & Sons Ltd.: New York, 1988; Vol *II*, pp 462−469.

(2) Berson, J. A. *Mol. Cryst. Liq. Cryst.* **1989**, *176*, 1−12.

(3) Borden, W. T.; Iwamura, H.; Berson, J. A. *Acc. Chem. Res.* **1994**, *27*, 109−116.

(4) Ovchinnikov, A. A. *Theor. Chim. Acta* **1978**, *47*, 297−303.

(5) Klein, D. J. *Pure Appl. Chem.* **1983**, *55*, 299−306.

(6) Borden, W. T.; Davidson, E. R. *J. Am. Chem. Soc.* **1977**, *99*, 4587−4594.

(7) Yuen, J. D.; Wang, M.; Fan, J.; Sheberla, D.; Kemei, M.; Banerji, N.; Scarongella, M.; Valouch, S.; Pho, T.; Kumar, R.; Chesnut, E. C.; Bendikov, M.; Wudl, F. *J. Polym. Sci., Part A: Polym. Chem.* **2015**, *53*, 287−293.

(8) Rajca, A. *Chem. - Eur. J.* **2002**, *8*, 4834−4841.

(9) Fukaminato, T.; Hirose, T.; Doi, T.; Hazama, M.; Matsuda, K.; Irie, M. *J. Am. Chem. Soc.* **2014**, *136*, 17145−17154.

(10) Matsuda, K.; Irie, M. *J. Am. Chem. Soc.* **2000**, *122*, 7195−7201.

(11) Sugawara, T.; Matsushita, M. M. *J. Mater. Chem.* **2009**, *19*, 1738−1753.

(12) Herrmann, C.; Solomon, G. C.; Ratner, M. A. *J. Chem. Phys.* **2011**, *134*, 224306−9.

(13) Shultz, D. A.; Kirk, M. L. *Chem. Commun.* **2014**, *50*, 7401−7402ff.

(14) Seeger, D. E.; Berson, J. A. *J. Am. Chem. Soc.* **1983**, *105*, 5146−5147.

(15) Izuoka, A.; Hiraishi, M.; Abe, T.; Sugawara, T.; Sato, K.; Takui, T. *J. Am. Chem. Soc.* **2000**, *122*, 3234−3235.

(16) Ravat, P.; Ito, Y.; Gorelik, E.; Enkelmann, V.; Baumgarten, M. *Org. Lett.* **2013**, *15*, 4280−4283.

(17) Hui, P.; Chandrasekar, R. *Adv. Mater.* **2013**, *25*, 2963−2067.

(18) Ali, Md. E.; Datta, S. N. *J. Phys. Chem. A* **2006**, *110*, 13232−13237.

(19) Akpinar, H.; Schlueter, J. A.; Lahti, P. M. *Chem. Commun.* **2013**, *49*, 3345−3347.

(20) Morgan, G. T.; Coulson, E. A. *J. Chem. Soc.* **1929**, *0*, 2203−2214.

(21) Staab, H. A.; Sauer, M. *Liebigs Ann. Chem.* **1984**, *1984*, 742−760.

(22) Schwab, M. G.; Hamburger, M.; Feng, X.; Shu, J.; Spiess, H. W.; Wang, X.; Antonietti, M.; Müllen, K. *Chem. Commun.* **2010**, *46*, 8932−8934.

(23) Ovcharenko, V.; Fokin, S.; Rey, P. *Mol. Cryst. Liq. Cryst. Sci. Technol., Sect. A* **1999**, *334*, 109−119.

(24) Catala, L.; Le Moigne, J.; Kyritsakas, N.; Rey, P.; Novoa, J. J.; Turek, P. *Chem. - Eur. J.* **2001**, *7*, 2466−2480.

(25) Ichimura, T.; Doi, K.; Mitsuhashi, C.; Ishida, T.; Nogami, T. *Polyhedron* **2003**, *22*, 2557−2564.

(26) Mann, C.; Gompper, R.; Polborn, K. *Cambridge Structure Database Code FOGKAO*, 2004.

(27) Akpinar, H.; Schlueter, J. A.; Lahti, P. M. *CrystEngComm* **2014**, *16*, 5832−5838.

(28) Kirste, B. *Anal. Chim. Acta* **1992**, *265*, 191−200.

(29) Kanzaki, Y.; Shiomi, D.; Sato, K.; Takui, T. *J. Phys. Chem. B* **2012**, *116*, 1053−1059.

(30) Lahti, P. M.; Rossi, A. R.; Berson, J. A. *J. Am. Chem. Soc.* **1985**, *107*, 2273−2280.

(31) Frisch, M. J.; et al. *Gaussian 09*, revision B.01 ed.; Gaussian, Inc: Wallingford CT, 2010. A full author list citation is given in the Supporting Information.

(32) Grimme, S.; Ehrlich, S.; Goerigk, L. *J. Comput. Chem.* **2011**, *32*, 1456−65.

(33) Yamaguchi, K.; Jensen, F.; Dorigo, A.; Houk, K. N. *Chem. Phys. Lett.* **1988**, *149*, 537−542.

(34) Lee, C.; Yang, W.; Parr, R. G. *Phys. Rev. B: Condens. Matter Mater. Phys.* **1988**, *37*, 785−789.

(35) Becke, A. D. *J. Chem. Phys.* **1993**, *98*, 5648−5.

(36) Ling, C.; Minato, M.; Lahti, P. M.; van Willigen, H. *J. Am. Chem. Soc.* **1992**, *114*, 9959−9966.

(37) Bleaney, B.; Bowers, K. D. *Proc. R. Soc. London, Ser. A* **1952**, *214*, 451−465.

(38) Yoshizawa, K. Orbital Interactions Determining the Exchange Effects in Organic Molecular Crystals. In *Magnetic Properties of Organic Materials*; Lahti, P. M., Ed.; Marcel-Dekker: New York, NY, 1999.

(39) Heise, H.; Köhler, F.; Mota, F.; Novoa, J. J.; Veciana, J. *J. Am. Chem. Soc.* **1999**, *121*, 9659−9667.

(40) Seber, G.; Freitas, R. S.; Oliveira, N. F., Jr.; Lahti, P. M. *Cryst. Growth Des.* **2013**, *13*, 893−900.

DOI: 10.1021/acs.cgd.6b00588
Cryst. Growth Des. 2016, 16, 4051−4059